Available online at www.sciencedirect.com

ScienceDirect

JOURNAL OF IRON AND STEEL RESEARCH, INTERNATIONAL. 2007, 14(5): 07-12, 30

Mathematical Model for Electroslag Remelting Process

DONG Yan-wu[1], JIANG Zhou-hua[1], LI Zheng-bang[2]

(1. School of Materials and Metallurgy, Northeastern University, Shenyang 110004, Liaoning, China;
2. Institute for Metallurgical Technology, Central Iron and Steel Research Institute, Beijing 100081, China)

Abstract: A mathematical model, including electromagnetic field equation, fluid flow equation, and temperature field equation, was established for the simulation of the electroslag remelting process. The distribution of temperature field was obtained by solving this model. The relationship between the local solidification time and the interdendritic spacing during the ingot solidification process was established, which has been regarded as a criterion for the evaluation of the quality of crystallization. For a crucible of 950 mm in diameter, the local solidification time is more than 1 h at the center of the ingot with the longest interdendritic spacing, whereas it is the shortest at the edge of the ingot according to the calculated results. The model can be used to understand the ESR process and to predict the ingot quality.

Key words: electroslag; remelting; mathematical model; interdendritic spacing; local solidification time

Symbol List

C_1, C_2——Constants in κ-ε model;
C_d——Dissipation rate constant;
c_P——Specific heat;
d——Interdendritic spacing, m;
G——Generation term for turbulence kinetic energy;
g——Gravitational acceleration, $(\mathrm{m \cdot s^{-2}})$;
H——Magnetic field intensity, $(\mathrm{A \cdot m^{-1}})$;
$\tilde{H}$——Complex amplitude of H;
$\tilde{H}_r$, $\tilde{H}_\theta$, $\tilde{H}_z$——Magnetic field intensity in r, θ, and z direction, respectively;
h_{sw}——Overall heat transfer coefficient between slag and cooling water, $(\mathrm{W \cdot m^{-2} \cdot K^{-1}})$;
$h_{w,i}$——Heat transfer coefficient of other position, $(\mathrm{W \cdot m^{-2} \cdot K^{-1}})$;
I_0——Reference value of current, A;
J——Current intensity, $(\mathrm{A \cdot m^{-1}})$;
$\tilde{J}$——Complex amplitude of J;
$\bar{\tilde{J}}_r$——Complex conjugation of $\tilde{J}$;
k_1, k_2——Coefficient, depending on steel grade;
k_{eff}——Effective thermal conductivity, $(\mathrm{W \cdot m^{-1} \cdot K^{-1}})$;
Q_s——Rate of heat extraction from slag by metal droplets;
q_r——Radiant heat loss, J;
R——Radius, m;
r——Radial coordinate, m;
T——Temperature;
t——Time, s;
v_c——Solidification rate of ingot, $(\mathrm{m \cdot h^{-1}})$;
v_r, v_z——Velocity of r and z direction, $(\mathrm{m \cdot h^{-1}})$;
z——Axial coordinate, m;
z_S, z_L——Position of solidus and liquidus, m;
β——Coefficient of thermal expansion of slag;
ξ——Vorticity;
ψ——Stream function;
κ——Kinetic energy of turbulence;
ε——Dissipation rate of turbulence energy;
ρ——Density, $(\mathrm{kg \cdot m^{-3}})$;
σ——Electrical conductivity, $(\Omega^{-1} \cdot \mathrm{m^{-1}})$;
ω——Angular frequency of current, $(\mathrm{rad \cdot s^{-1}})$;
μ——Viscosity of slag, $(\mathrm{Pa \cdot s^{-1}})$;
μ_0——Magnetic permeability, $(\mathrm{H \cdot m^{-1}})$;
μ_{eff}——Effective viscosity, $(\mathrm{Pa \cdot s^{-1}})$;
μ_t——Turbulent viscosity;
Subscript
e——Electrode;
i——Ingot;
L——Metal pool;
m——Mushy zone;
s——Liquid slag.

Foundation Item: Item Sponsored by Weaponry Pre-Research Fund (51412020304QT0901)
Biography: DONG Yan-wu(1978-), Male, Doctor Candidate; **E-mail**: yanwu_dong@163.com; **Revised Date**: November 29, 2006

The ingot structure is a main objective to be controlled for electroslag remelting process, which determines the properties of the final steel products. A model for describing the ingot thermal field established in previous study[1] was not concerned with the thermal field of electrode, liquid slag, etc. However, all these thermal fields exist in the system, which should be considered in the model. As it is known, the electrode remelting process is a very complex system, involving electromagnetic fields, fluid flow phenomena, heat transfer, etc. , which should be also considered in the simulation. The proper statement of the problem requires the definition of both the appropriate fluid flow equations and electromagnetic field equations. Ultimately these equations should be coupled with a heat-balance equation. In several earlier studies[2-5], the turbulent Navier-Stokes equations and thermal transfer equations were presented through the statement of Maxwell's equations, which described the velocity fields, electromagnetic fields, and temperature fields. In present study, a model involving electromagnetic fields, fluid flow, and thermal fields was established and temperature fields in the system was particularly emphasized as evaluation index of the model accuracy. Ballantyne[6] showed that the ingot structure is controlled by the local solidification time (*LST*) rather than by the pool profile. *LST* can never be obtained by measurement, but it can be achieved by calculation. However, till now, there is less model that can be used to calculate the *LST*. Moreover, *LST* in ingot can be used to calculate the interdendritic spacing, which is a criterion to assess an ingot quality. The purpose of the study is to establish predictive relationships among current input, pool profiles, *LST*, and interdendritic spacing for ESR process.

The study to be described is based on the following assumptions:

(1) Cylindrical symmetry about the centerline;

(2) Slag-electrode and slag-metal boundaries are presented by horizontal surfaces;

(3) Quasi-steady state;

(4) The effect of metal droplets on the motion of the slag is neglected;

(5) Voltage loss is only in the molten slag pool;

(6) Continuity of heat flux at all the external surfaces and at the slag-metal interface;

(7) The tip of the electrode is the liquidus temperature;

(8) The electrode and ingot are the infinite long conductor.

1 Mathematical Model

To calculate the temperature fields in the system, first, the Maxwell's equations to compute the electromagnetic force field and the turbulent Navier-Stokes equations to calculate the fluid flow should be solved. These equations influence each other. The physical concept used in the development of the mathematical model of the process is sketched in Fig. 1.

1.1 Transport equation for magnetic fields and boundary conditions

The magneto-hydrodynamic form of Maxwell's equations should be solved to calculate the electromagnetic force field. The transport equation for the magnetic field takes the following form at cylindrical symmetry[2,4,5,7,8]:

$$\frac{1}{r}\frac{\partial}{\partial r}\left[r\frac{\partial \widehat{H}_\theta}{\partial r}\right]+\frac{\partial^2 H_\theta}{\partial z^2}=j\sigma\omega\mu_0\,\widehat{H}_\theta \tag{1}$$

where $j=\sqrt{-1}$, and the boundary conditions for Eqn. (1) are expressed using the following physical constraints:

$$\frac{\partial \widehat{H}_\theta}{\partial z}=0 \qquad (0\leqslant r\leqslant R_e,\ z=0);$$

$$\widehat{H}_\theta=\frac{I_0}{2\pi R_e} \qquad (r=R_e,\ 0\leqslant z\leqslant z_1);$$

$$\widehat{H}_\theta=\frac{I_0}{2\pi r} \qquad (R_e\leqslant r\leqslant R_m,\ z=z_1);$$

$$\widehat{H}_\theta=\frac{I_0}{2\pi R_i} \qquad (r=R_m,\ z_1\leqslant z\leqslant z_6);$$

$$\frac{1}{\sigma_e}\left[\frac{\partial \widehat{H}_\theta}{\partial r}+\frac{\widehat{H}_\theta}{r}\right]_e=\frac{1}{\sigma_s}\left[\frac{\partial \widehat{H}_\theta}{\partial r}+\frac{\widehat{H}_\theta}{r}\right]_s$$
$$(r=R_e,\ z_1<z<z_2);$$

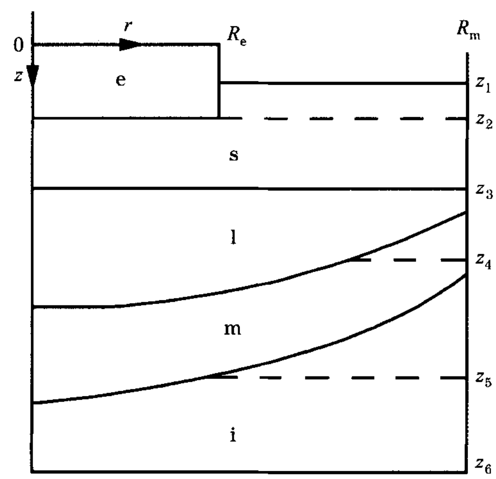

Fig. 1 Physical concept of process model

$$\frac{1}{\sigma_e}\left(\frac{\partial \widehat{H}_\theta}{\partial z}\right)_e=\frac{1}{\sigma_s}\left(\frac{\partial \widehat{H}_\theta}{\partial z}\right)_s \qquad (0\leqslant r\leqslant R_e,\ z=z_2);$$

$$\left(\frac{\partial \widehat{H}_\theta}{\partial z}\right)_s=\frac{\sigma_s}{\sigma_L}\left(\frac{\partial \widehat{H}_\theta}{\partial z}\right)_L \qquad (0<r<R_m,\ z=z_3);$$

$$\frac{\partial \widehat{H}_\theta}{\partial z}=0 \qquad (0<r<R_m,\ z=z_6);$$

$$\widehat{H}_\theta=0 \qquad (r=0,\ 0\leqslant z\leqslant z_6).$$

1.2 Fluid flow equation and boundary conditions

Fluid flow, driven by electromagnetic force, buoyancy, etc., is an important phenomenon in ESR system. Electromagnetic force field plays the major role in the fluid flow. The equation of fluid flow may be given as the vortex transport equation in axi-symmetric[2,7,9] cylindrical coordinate system, which takes the following form:

$$r^2\left[\frac{\partial}{\partial z}\left(\frac{\xi}{r}\cdot\frac{\partial\psi}{\partial r}\right)-\frac{\partial}{\partial r}\left(\frac{\xi}{r}\cdot\frac{\partial\psi}{\partial z}\right)\right]-\frac{\partial}{\partial z}\left[r^3\cdot\frac{\partial}{\partial z}\left(\mu_{\rm eff}\cdot\frac{\xi}{r}\right)\right]-\frac{\partial}{\partial r}\left[r^3\frac{\partial}{\partial r}\left(\mu_{\rm eff}\cdot\frac{\xi}{r}\right)\right]-r\left[\mu_0{\rm Re}(\widehat{H}_\theta\bar{J}_r)+r\rho\beta g\left(\frac{\partial T}{\partial r}\right)\right]=0 \qquad (2)$$

For cylindrical coordinate, ξ and ψ can be defined as the following form:

$$\xi=\frac{\partial v_r}{\partial z}-\frac{\partial v_z}{\partial r} \qquad (3)$$

$$v_r=-\frac{1}{\rho r}\frac{\partial\psi}{\partial z} \qquad (4)$$

$$v_z=-\frac{1}{\rho r}\frac{\partial\psi}{\partial r} \qquad (5)$$

The relationship between ξ and ψ may be expressed as follows:

$$\xi+\frac{\partial}{\partial z}\left(\frac{1}{\rho r}\frac{\partial\psi}{\partial z}\right)+\frac{\partial}{\partial r}\left(\frac{1}{\rho r}\frac{\partial\psi}{\partial r}\right)=0 \qquad (6)$$

By solving the κ-ε model, the turbulent viscosity can be calculated. The equation of κ-ε function can be expressed as follows:

$$\frac{\partial}{\partial z}\left(\phi\frac{\partial\psi}{\partial z}\right)-\frac{\partial}{\partial r}\left(\phi\frac{\partial\psi}{\partial z}\right)-\frac{\partial}{\partial z}\left(r\frac{\mu_{\rm eff}\partial\phi}{\sigma_\phi\partial z}\right)-\frac{\partial}{\partial r}\left(r\frac{\mu_{\rm eff}\partial\phi}{\sigma_\phi\partial r}\right)-rS_\phi=0 \qquad (7)$$

where $\phi=\kappa$ or ε;

$$S_\kappa=2\mu_t\left[\left(\frac{\partial v_z}{\partial z}\right)^2+\left(\frac{\partial v_r}{\partial r}\right)+\left(\frac{v_r}{r}\right)^2+\frac{1}{2}\left(\frac{\partial v_r}{\partial z}+\frac{\partial v_z}{\partial r}\right)^2\right]-\rho\varepsilon \qquad (8)$$

$$S_\varepsilon=C_1\frac{\varepsilon}{\kappa}G-C_2\rho\frac{\varepsilon^2}{\kappa} \qquad (9)$$

$$\mu_{\rm eff}=\mu+C_d\rho\kappa^2/\varepsilon \qquad (10)$$

The boundary conditions for fluid flow satisfy the following physical constraints:

$$\psi=\frac{\partial\kappa}{\partial r}=\frac{\partial\varepsilon}{\partial r}=0 \qquad (r=0,\ z_2\leqslant z\leqslant z_3);$$

$$\psi=\frac{\xi}{r}=\frac{\partial\kappa}{\partial z}=\frac{\partial\varepsilon}{\partial z}=0 \qquad (z=z_1,\ R_e\leqslant r\leqslant R_m);$$

$$\psi=\kappa=\varepsilon=0 \qquad (z=z_2,\ 0\leqslant r\leqslant R_e);$$

$$\psi=\kappa=\varepsilon=0,\ \left(\frac{\xi}{r}\right)_0=\frac{3(\psi_0-\psi_1)}{\rho_s r^2(z_1-z_0)^2}-\frac{1}{2}\left(\frac{\xi}{r}\right)_1 \qquad (z=z_3,\ 0\leqslant r\leqslant R_m);$$

$$\psi=\kappa=\varepsilon=0 \qquad (r=R_e,\ z_1\leqslant z\leqslant z_2);$$

$$\psi=\kappa=\varepsilon=0 \qquad (r=R_m,\ z_1\leqslant z\leqslant z_3).$$

1.3 Governing equation for temperature field

By the coupling of the electromagnetic fields and fluid-flow equations, the governing equations for temperature fields can be expressed in the following form at cylindrical coordinate:

$$r\rho c_P v_c\frac{\partial T}{\partial z}+c_P\left[\frac{\partial}{\partial z}\left(T\frac{\partial\psi}{\partial r}\right)-\frac{\partial}{\partial r}\left(T\frac{\partial\psi}{\partial z}\right)\right]=\frac{\partial}{\partial r}\left(k_{\rm eff}r\frac{\partial T}{\partial r}\right)+\frac{\partial}{\partial z}\left(k_{\rm eff}r\frac{\partial T}{\partial z}\right)+rS_T \qquad (11)$$

where S_T is source term for temperature equation.

At the same time, the thermal transfer equations of electrode, metal pool, mushy zone, and ingot region takes the following form at cylindrical coordinate:

$$r_i\rho_i c_{P,i}v_i\frac{\partial T}{\partial z}=\frac{\partial}{\partial r}\left(K_i r\frac{\partial T}{\partial r}\right)+\frac{\partial}{\partial z}\left(K_i r\frac{\partial T}{\partial z}\right)+rS_{T,i} \qquad (12)$$

The physical constraints for Eqn. (11) and Eqn. (12) are as follows:

$$\frac{\partial T}{\partial r}=0 \qquad (r=0,\ 0\leqslant z\leqslant z_6);$$

$$\frac{\partial T}{\partial z}=0 \qquad (z=0,\ 0\leqslant r\leqslant R_e \text{ and } z=z_6,\ 0\leqslant r\leqslant R_m);$$

$$k_{\rm eff}\frac{\partial T}{\partial z}\Big|_s=q_r \qquad (z=z_1,\ R_e\leqslant r\leqslant R_m);$$

$$k\frac{\partial T}{\partial r}\Big|_e=k\frac{\partial T}{\partial r}\Big|_s \qquad (r=R_e,\ z_1\leqslant z\leqslant z_2);$$

$$T=T_{m,e} \qquad (z=z_2,\ 0\leqslant r\leqslant R_e);$$

$$-k_{\rm eff}\frac{\partial T}{\partial z}\Big|_s+\frac{Q_s}{\pi R_e^2}\chi=-k_L\frac{\partial T}{\partial z}\Big|_L$$

$(z=z_3,\ 0\leqslant r\leqslant R_m)$, $[\chi=1$, when $r\leqslant R_e$, and $\chi=0$, when $r>R_e]$;

$$T=T_{L,s},\ -k\frac{\partial T}{\partial r}\Big|_s=h_{w,s}(T-T_w) \qquad (r=R_m,\ z_1\leqslant z\leqslant z_3);$$

$$-k\frac{\partial T}{\partial r}\Big|_i=h_{w,i}(T-T_w) \qquad (r=R_m,\ z_3\leqslant z\leqslant z_6).$$

1.4 Calculation of *LST* and relationship between *LST* and quality of ingot

By solving the above equations, the distribution of temperature in the system can be obtained, and then the liquidus and solidus curves in ingot are determined. *LST* can be calculated using Eqn. (13).

$$LST=(z_s-z_L)/v_c \quad (13)$$

$$\lg d=k_1+k_2\lg LST \quad (14)$$

Consequently Eqn. (14) that was represented by Flemings regarding the relationship of *LST* and interdendritic spacing will be used to calculate the interdendritic spacing, which will be used to assess the ingot quality.

2 Numerical Solution of Governing Equations

The model was used in a 10-ton ESR system. The crucible size of the 10-ton ESR furnace was ϕ950 mm×2 400 mm and the size of electrode was ϕ680 mm×3 400 mm.

The governing equations were solved using a Gauss-Seidel method. The system was divided into 421×327 grids and the molten slag under the electrode had the largest grid density. Models were solved with Window's operating platform, at Visual Basic 6.0 for programming tools and the calculating precision was 0.005. Fig. 2 is the simplified flow diagram for the computational scheme.

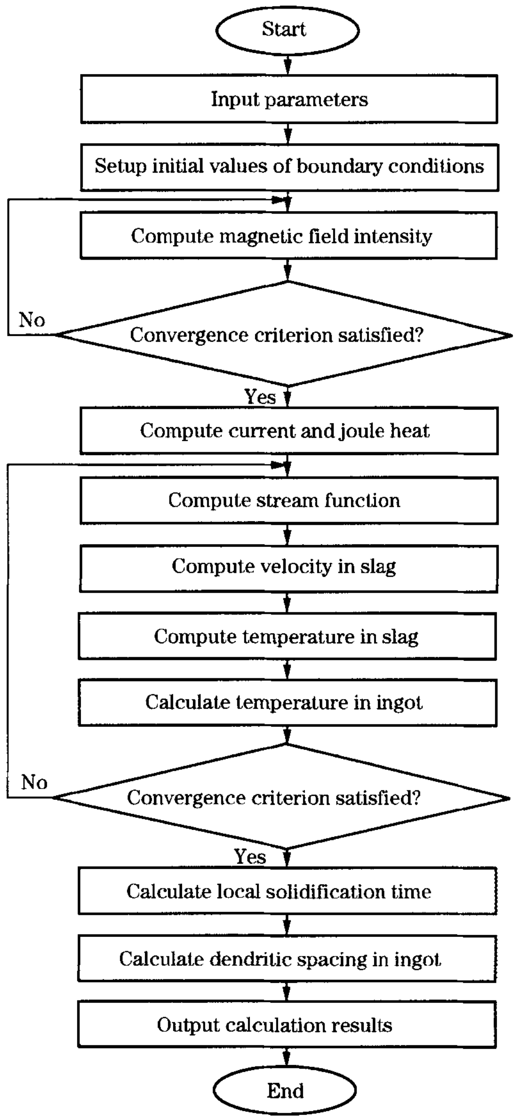

Fig. 2 Simplified flow diagram for computational scheme

3 Computed Results

The final aim of this study is to obtain the temperature distribution of the ESR system, so the temperatures of electrode and slag were measured to check the accuracy of the model. A 10-ton industrial-scale ESR with the core of descending power control was calculated using the model established above. A slag containing CaF_2 of 60%, Al_2O_3 of 20%, and CaO of 20% was used. A NiCr-NiSi thermocouple with protecting tube was used to measure the temperature of the electrode surface. The temperature in electrode was approximately partitioned into two segments and there was a distinct turning point between the two parts. Fig. 3 shows the calculated and measured surface temperature of electrode. The results indicated that the surface temperature of electrode away from the molten slag surface is lower than that of the nearby liquid slag surface. Simultaneously, the temperature gradient was found to be lower at the surface than the bottom nearby the molten slag. The error obtained from the measured and calculated results is less than 10 ℃.

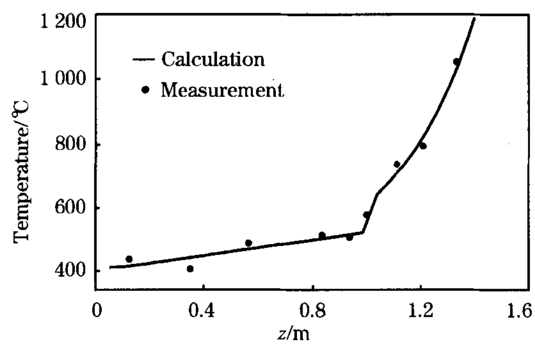

Fig. 3 Calculated and measured surface temperature of electrode

As the slag contains excessive CaF_2, which erodes most ceramic materials, a W3RE-W25RE thermocouple with the graphite protecting tube was used to measure the temperature of liquid slag. It is very difficult to measure the temperature under the electrode; therefore, only the temperature of three positions between the electrode and cooled water copper was considered. Fig. 4 shows the calculated and measured temperature in the molten slag. The temperature of slag free surface reduced gradually from the position of nearby electrode to the position of nearby crucible. The position of nearby cooled water copper had the lowest temperature, about 1 342 ℃, in term of the measured result, which is approximate to the result of 1 330 ℃ obtained in Ref. [10]. From the surface to the interior of the slag, the temperature increased, and the temperature gradient nearby the surface is larger than that of the interior, as is also similar to the results in Ref. [10]. The calculated results are very accurate as shown in Fig. 3 and Fig. 4.

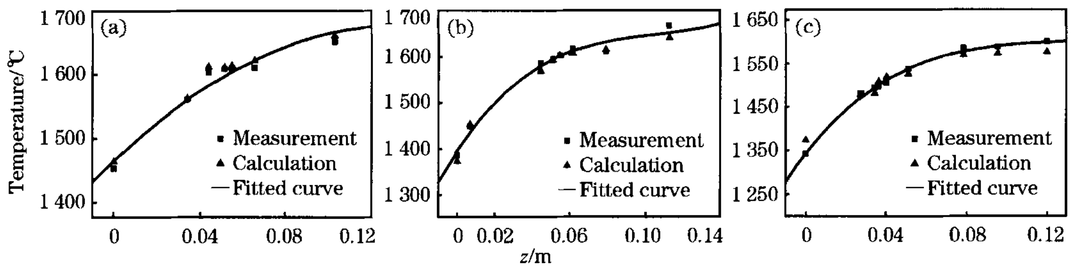

(a) Nearby electrode; (b) Between electrode and crucible; (c) Nearby crucible

Fig. 4 Calculated and measured temperature in slag

Generally, it is absolutely necessary to determine the liquidus and solidus curves in ingot, which determined the directions and quality of crystal to some extent. Fig. 5 shows the distribution of temperature in the zones of metal pool and ingot. The liquidus and solidus positions are relatively shallow at the edge of ingot, whereas they are deep at the center of the ingot. The shapes of other isotherms are similar to those of the liquidus and solidus isotherms.

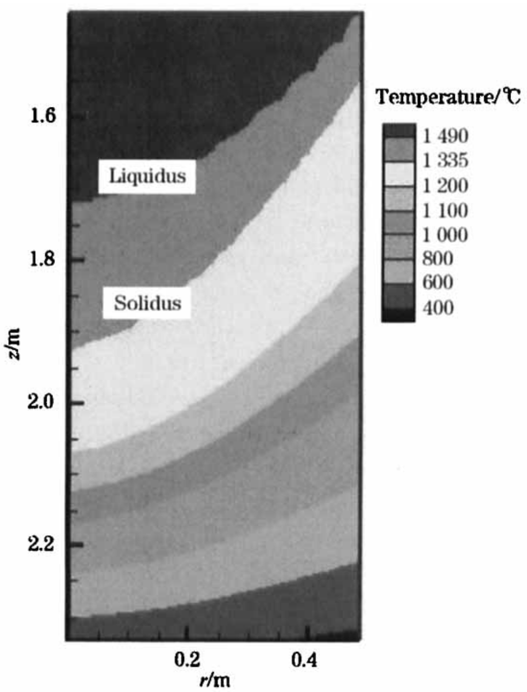

Fig. 5 Calculated temperature distribution in ingot

The lowest temperature exists at the bottom of the ingot, which has the largest cooling power.

In Fig. 6, the curves 1 to 7 are the liquidus and solidus curves at different time interval. With the increase in the height of the ingot, the cooling capacity decreases, and this induces the increase in metal pool depth. The crystallization direction of ingot is determined by the shape of metal pool, and thus, researchers seek the method to control the shape of metal pool through adjusting the various influencing factors especially the voltage and current all the times. The cooling capacity in ingot center is

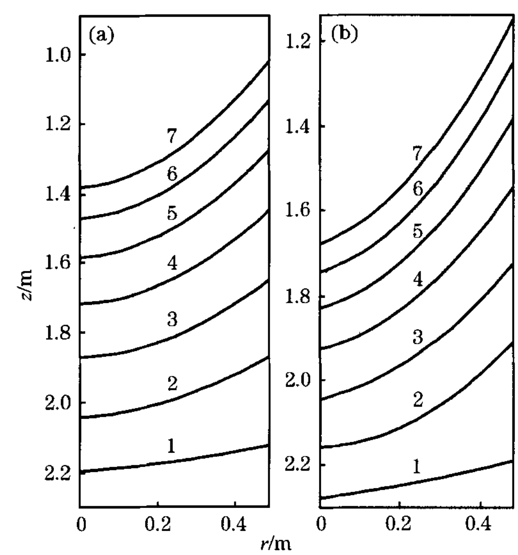

Fig. 6 Liquidus curve (a) and solidus curve (b) for various height of ingot in remelting process

the worst where the depth of metal pool is relatively deeper than other positions, which results in the longest *LST* in ingot center.

The *LST* in the process of metal solidification has a close relation with the interdendritic spacing that determines the crystallization quality to some extent. Fig. 7 shows the relationship between the *LST* and the interdendritic spacing. In Fig. 7, the longest *LST* is more than 1 h, which is a relatively longer time for the solidification process. With the decrease in *LST* from the center to the edge, the interdendritic spacing decreases. Furthermore, according to the general fact, it is found that the fine equiaxed crystal exists on the edge of ingot; however, the crystal grain is large in the center of ingot, so interdendritic spacing may be used to assess the solidification quality in ingot. Certainly, the standard of interdendritic spacing should be established by the discrete conditions including the steel grade, equipment, etc. Fig. 8 shows the compared results of interdendritic spacing obtained by calculating and measuring methods, which are very close.

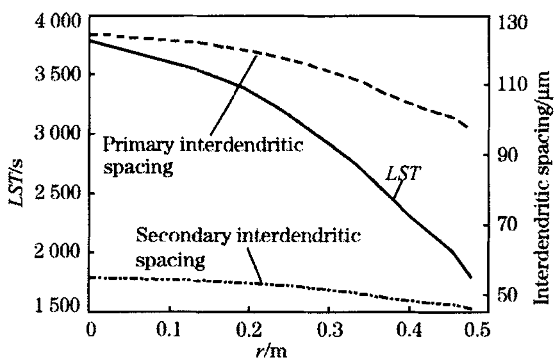

Fig. 7 Relationship between *LST* and interdendritic spacing

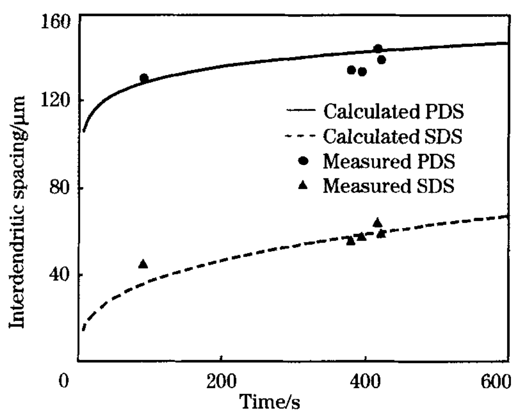

PDS—Primary interdendritic spacing;
SDS—Second interdendritic spacing

Fig. 8 Comparison of calculated results of interdendritic spacing with measured ones

It is well known that the voltage and current has significant effect on the ESR process that influences the interior quality of crystallization and ingot surface. Fig. 9 shows the influence of current on the liquidus and solidus position. The larger the input current, the deeper are the metal pool and mushy zone existing at the center of the ingot. It is known that power supply plays an important role in the ESR process. To ensure the product quality, an appropriate power supply should be provided.

Therefore, the model can be used to understand ESR process and to predict the ingot quality under the specific conditions.

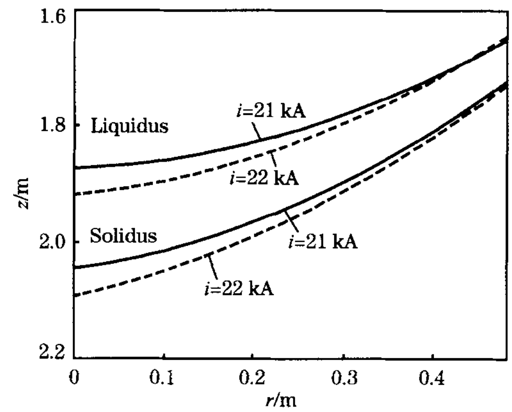

Fig. 9 Influence of current intensity on liquidus and solidus positions

4 Conclusions

(1) The results obtained by the model are in good agreement with those obtained from the measurement, and the model can be used to understand the ESR process and to predict the ingot quality under a specific condition.

(2) The calculated results of interdendritic spacing is accurate and the relationship between the local solidification and the interdendritic spacing can be used to assess the ingot quality.

(3) The temperature in electrode is partitioned into two segments where there is a distinct turning point between the two parts and the surface temperature of electrode away from the molten slag surface is lower than that of the nearby liquid slag surface.

(4) The input current plays an important role in the ESR process, which obviously influences the liquidus and solidus positions that determine the crystallization direction and quality to some extent. The larger the current, **(Continued on Page 30)**

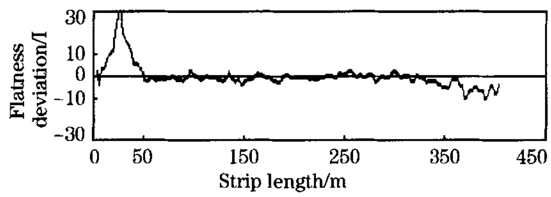

Fig. 2 Flatness deviation variation

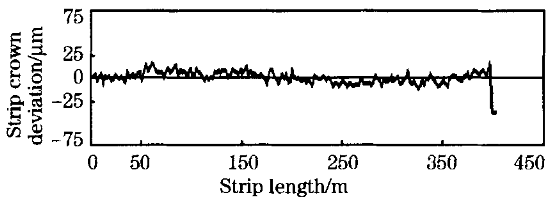

Fig. 3 Profile deviation variation

accuracy in ± 15 μm exceeds 97.79%.

5 Conclusions

Setup model calculates the mechanical actuator references and the feedback model provides the critical feedback to the dynamic control loops for improving predictions of the SSU model. The deviation of measured and target data shows that the strip flatness deviation and strip profile deviation could be controlled in the target scope of 98.79% and 97.79%, respectively. Further research on the SSU system for HSM is necessary to improve the setting accuracy.

References:

[1] ZHANG Jin-zhi. Development and Application of Shape Theory [J]. Metallurgical Equipment, 2001, (1): 1-5 (in Chinese).

[2] HOU Zhang-bao. Shape Control of Wide Hot-Strip [J]. Steel Rolling, 1995, (1): 45-48 (in Chinese).

[3] WANG Wen-ming, ZHONG Jue, TAN Jian-ping. Development of Strip Shape Control Theory and Technique [J]. Mining and Metallurgical Engineering, 2001, 21(4): 70-72 (in Chinese).

[4] Guo R M. Characteristics of Rolling Mills With Roll Shift [J]. Iron and Steel Engineer, 1988, 65(12): 45-56.

[5] Bald W, Beisemann G, Feldmann H, et al. Continuously Variable Crown (CVC) Rolling [J]. Iron and Steel Engineer, 1987, 64(3): 32-40.

[6] LIU Li-zhong, LV Cheng, ZHAO Qi-lin, et al. Development of Flatness Calculating Software for CVC Finishing Stands of HSM [J]. Research on Iron and Steel, 2000, (2): 28-31 (in Chinese).

[7] KONG Xiang-wei, YE He-zhou, XU Jian-zhong, et al. Offline Simulation of PFC for Hot Rolling Strip [J]. JMST, 2003, 19(5): 502-504.

[8] WANG Ying-rui, YUAN Jian-guang, LIU Hong-min. Shape Control Simulation on 4-High CVC Mill [J]. Journal of Iron and Steel Research, International, 2005, 12(2): 25-32.

[9] SUN Yi-kang. Models and Control for Hot Strip Mill [M]. Beijing, China: Metallurgical Industry Press, 2002 (in Chinese).

[10] Deshpande A S, Srinivasa Murthy K. Computer Analysis for the Prediction of a Strip Profile in Cold Rolling [J]. Journal of Materials Processing Technology, 1997, 63(1-3): 712-717.

(Continued From Page 12) the deeper is the metal pool. Therefore, proper parameters should be determined to ensure the product quality and to improve the productivity as high as possible.

References:

[1] Ballantyne A S, Mitchell A. Modelling of Ingot Thermal Fields in Consumable Electrode Remelting Processes [J]. Ironmaking and Steelmaking, 1977, 4(4): 222-239.

[2] Choudhary M, Szekely J. Modeling of Profiles, Temperature Profiles and Velocity Fields in ESR Systems [J]. Metallurgical Transactions, 1980, 11B(3): 439-453.

[3] Kelkar K M, Mok J, Patankar S V, et al. Computational Modeling of Electroslag Remelting Processes [J]. Journal de Physique IV, 2004, 120: 421-428.

[4] Dilawari A H, Szekely J. Heat Transfer and Fluid Flow Phenomena in Electroslag Refining [J]. Metallurgical Transactions, 1978, 9B(3): 77-87.

[5] Dilawari A H, Szekely J. A Mathematical Model of Slag and Metal Flow in the ESR Process [J]. Metallurgical Transactions, 1977, 8B(2): 227-236.

[6] Hernandez-Morales B, Mitchell A. Review of Mathematical Models of Fluid Flow, Heat Transfer, and Mass Transfer in Electroslag Remelting Process [J]. Ironmaking and Steelmaking, 1999, 26(6): 423-438.

[7] JIANG Zhou-hua. Mathematical Simulation and Experiment Analysis of Thermal Transfer for ESR [D]. Shenyang, China: Northeastern University Press, 1986 (in Chinese).

[8] WEI Ji-he, REN Yong-li. Mathematical Simulation of Magnetic Field in ESR System [J]. Acta Metallurgica Sinca, 1995, 31 (2): 51-60 (in Chinese).

[9] WEI Ji-he, REN Yong-li. Mathematical Modeling of Slag Flow Field in ESR System [J]. Acta Metallurgica Sinca, 1994, 30 (11): 481-490 (in Chinese).

[10] FU Jie, CHEN Chong-xi, CHEN En-pu, et al. Temperature Distribution Round the Molten Slag Pool in the Process of Electroslag Refining [J]. Acta Metallurgica Sinca, 1979, 15 (1): 44-50 (in Chinese).